Supplementary Information

A PHGDH inhibitor reveals coordination of serine synthesis and 1-carbon unit fate

Michael E. Pacold[1,2,3,4,5,6], Kyle R. Brimacombe[7], Sze Ham Chan[1,2,3,4,6], Jason M. Rohde[7], Caroline A. Lewis[3], Lotteke J.Y.M. Swier[1,2,3,4], Richard Possemato[8], Walter W. Chen[1,2,3,4,6], Lucas B. Sullivan[3], Brian P. Fiske[3], Sung Won Cho[1,2,3,4], Elizaveta Freinkman[1,2,3,4], Kıvanç Birsoy[9], Monther Abu-Remaileh[1,2,3,4], Yoav Shaul[1,2,3,4], Chieh Min Liu[1,2,3,4], Minerva Zhou[1,2,3,4], Min Jung Koh[1,2,3,4], Haeyoon Chung[1,2,3,4], Shawn M. Davidson[3], Alba Luengo[3], Amy Q. Wang[7], Xin Xu[7], Adam Yasgar[7], Li Liu[7], Ganesha Rai[7], Kenneth D. Westover[11], Matthew G. Vander Heiden[3], Min Shen[7], Nathanael S. Gray[5], Matthew B. Boxer[7], and David M. Sabatini[1,2,3,4]

[1]Whitehead Institute for Biomedical Research, 9 Cambridge Center, Cambridge, MA 02142, USA
[2]Howard Hughes Medical Institute, Department of Biology, Massachusetts Institute of Technology, Cambridge, MA 02139, USA
[3]Koch Institute for Integrative Cancer Research, 77 Massachusetts Avenue, Cambridge, MA 02139, USA
[4]Broad Institute of Harvard and Massachusetts Institute of Technology, 7 Cambridge Center, Cambridge, MA 02142, USA
[5]Dana-Farber Cancer Institute, Longwood Center, 350 Longwood Avenue, Boston, MA 02215, USA
[6]Department of Radiation Oncology, Dana-Farber Cancer Institute, 450 Brookline Avenue, Boston, MA 02215, USA
[7]National Center for Advancing Translational Sciences, National Institutes of Health, 9800 Medical Center Drive, Rockville, MD 20850, USA
[8]New York University Langone Medical Center, 550 First Avenue, MSB 504, New York, NY 10016, USA
[9]Laboratory of Metabolic Regulation and Genetics, The Rockefeller University, 1230 York Avenue, New York, NY 10065, USA
[10]Department of Biochemistry and Molecular Biology, The Institute for Medical Research Israel-Canada, The Hebrew University-Hadassah Medical School, Jerusalem 91120, Israel
[11]University of Texas Southwestern Medical Center, 5323 Harry Hines Boulevard, Dallas, TX 75390, USA

e-mail: sabatini@wi.mit.edu

Supplementary Results

Supplementary Table 1. Small molecule screening data

Category	Parameter	Description
Assay	Type of assay	In vitro, coupled
	Target	3-phosphoglycerate dehydrogenase (PHGDH)
	Primary measurement	Detection of resorufin using ViewLux reader: Resorufin fluorescence (ex525/em598, using delta between T0 and T20 min)
	Key reagents	PHGDH, PSAT1, PSPH, Diaphorase, resazurin, 3-PG, glutamate
	Assay protocol	Methods, Enzyme assays Primary PHGDH assay: 1 Dispense: 3 uL substrate/coupling reagent 2 Pintool compound transfer (23 nL in DMSO) 3 Dispense: 1 uL PHGDH/NAD+ reagent 4 Detection (initial read): resorufin fluorescence read in PerkinElmer ViewLux (ex525/em598) 5 Incubation: 20 min room temperature 6 Detection (final read): resorufin fluorescence read in PerkinElmer ViewLux (ex525/em598) Plates:Greiner black solid medium-binding 1536-well Assay buffer: 50 mM TEA pH 8.0, 10 mM $MgCl_2$, 0.05% BSA, 0.01% Tween-20 Substrate/coupling reagent:0.625 mM L-glutamate, 0.1 mM resazurin, 0.05 mM 3-PG, 500 nM PSAT1, 500 nM PSPH, 0.1 mg/mL diaphorase in assay buffer PHGDH/NAD+ reagent: 0.15 mM NAD+, 10 nM PHGDH in assay buffer Data normalization: Delta RFUs were calculated between T20min and T0min reads and normalized to control wells on each plate. 1x and 0x PHGDH control wells were used to normalize compound responses to 100% and 0% PHGDH activity, respectively.
	Additional comments	
Library	Library size	~400,000
	Library composition	Curated; known bioactives, non-commmercial compounds, natural products, diversity compounds, targeted libraries
	Source	NIH Molecular Libraries Small Molecule Repository (MLSMR)
	Additional comments	http://mli.nih.gov/mli/compound-repository/mlsmr-compounds/
Screen	Format	1536-well plates; quantitative HTS
	Concentration(s) tested	4 pt; 0.46 to 57uM; 5-fold dilution
	Plate controls	+/- PHGDH
	Reagent/ compound dispensing system	BioRAPTR
	Detection instrument and software	ViewLux
	Normalization	0% = DMSO neutral; 100% inhibition = no enzyme control
	Assay validation/QC	Z'-factor = 0.71; CV (%) = 4.8
	Additional comments	The primary screen was run on NIH/NCATS screening robotic system, please see details in http://www.ncbi.nlm.nih.gov/pmc/articles/PMC2651822/
Post-HTS analysis	Hit criteria	Compounds in curve classes -1.1, -1.2, -2.1 and -2.2 with efficacy greater than 50%
	Hit rate	0.3%
	Additional assay(s)	Uncoupled PHGDH assay; PHGDH assay with direct NADH detection; diaphorase counterscreen; GAPDH and LDHA counterscreens
	Confirmation of hit purity and structure	In the confirmation and counter assays, fresh stocks of the primary screening hits were QC'ed and re-plated on 1536-

Additional comments	well plates. These compounds were then re-tested in the hit validation assays using 11 point titrations with concentration ranging from 57 μM to 1 nM with 1:3 dilution.

Supplementary Fig.1. SAR, ADME and specificity data for PHGDH inhibitors

a

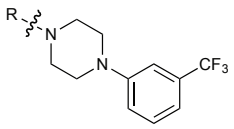

Entry	R	IC_{50}[a]	%inhibition[b]
1	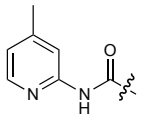	NA	16 (max)
2	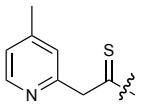	39	37
3	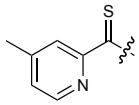	NA	9 (max)
4	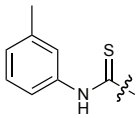	NA	20 (max)
5	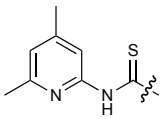	6.5	88

[a] IC_{50} determined in diaphorase coupled assay
[b] % inhibition is enzyme inhibition at 57 μM of compound

b *In vitro* ADME

Assay	Subtype	units	NCT-502	NCT-503
Buffer Stability	PHGDH assay buffer (with EDTA)	% remaining at 48 hours	>95 (n=1)	>95 (n=1)
	Aq. buffered 5 mM Glutathione		76 (n=1)	>95 (n=1)
	Aq. buffered 500 uM DTT		>95 (n=1)	>95 (n=1)
Liver Microsomal Stability	Mouse	% remaining at 15 minutes	70.2 ± 0.7 (n=2)	95.2 ± 4.3 (n=2)
	Rat		94.6 ± 5.4 (n=2)	104.9 ± 15.0 (n=2)
	Human		96.6 ± 0.4 (n=2)	98.4 ± 7.3 (n=2)
Passive Permeability	PAMPA	$x10^{-6}$ cm/s	935 ± 264 (n=9)	Equilibrium (n=8)
MDCK MDR1 Permeability	A-B	$x10^{-6}$ cm/s	10.0 ± 1 (n=3)	4.1 ± 0.7 (n=3)
	B-A		8.9 ± 0.9 (n=3)	5.7 ± 1.0 (n=3)
	Efflux ratio	fold	0.9	1.4
Aqueous Solubility		μM	1.23 ± 1.18 (n=8)	24.5 ± 2.5 (n=8)

c

	IC_{50} (μM)		
Enzyme	Inactive	NCT-502	NCT-503
PHGDH	>57	3.7	2.5
GAPDH	>100	>100	>100
LDHA	>57	>57	>57
HSD17B4	>57	>57	>57
GPD1	>100	>100	>100
GPD1L	>100	>100	>100

d

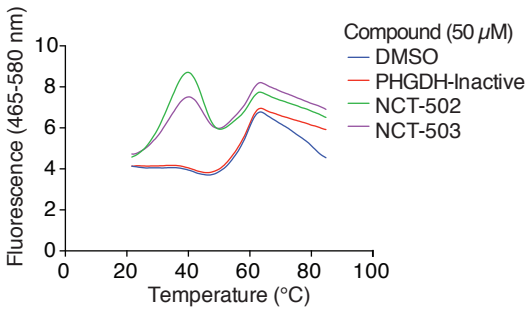

Supplementary Figure 1 | SAR, ADME and specificity data for PHGDH Inhibitors. (**a**) SAR of PHGDH inhibitors to improve potency and % inhibition. (**b**) In vitro ADME of NCT-502 and NCT-503. (c) Counterscreening data for NCT-502, NCT-503, and PHGDH-inactive. The compounds exhibit no significant activity against dehydrogenases in glycolysis. (**d**) Raw melting temperature data for PHGDH in the presence of DMSO (vehicle) or inhibitors.

Supplementary Fig.2. Additional target engagement and PK data for PHGDH inhibitors

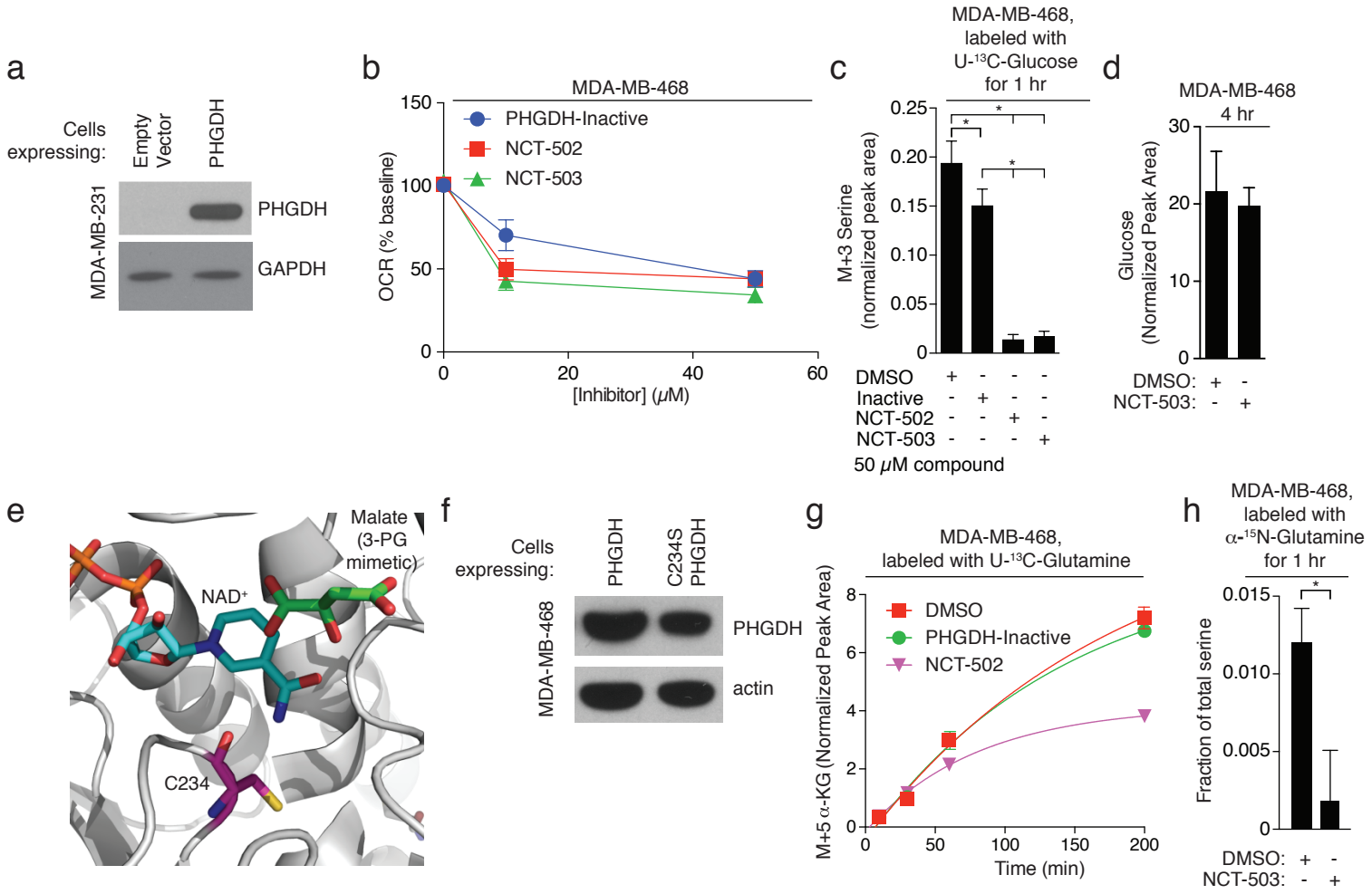

Supplementary Figure 2 | Additional target engagement and PK data for PHGDH inhibitors. All data points are the mean of three biological replicates unless otherwise specified. Error bars represent standard deviations. *, $p<0.05$, Student's *t*-test. (**a**). Ectopic expression of PHGDH in MDA-MB-231 breast cancer cells. Full gels are in Supplementary Fig. 8a. (**b**) Both active and inactive PHGDH inhibitors decrease oxygen consumption rates in MDA-MB-468 cells. (**c**) NCT-502 and NCT-503 decrase M+3, ^{13}C-labeled serine production from U-^{13}C glucose in MDA-MB-468 cells. Inactive compound does not greatly decrease M+3 labeled serine production from U-^{13}C glucose. (**d**) NCT-503 does not change intracellular glucose concentrations in MDA-MB-468 cells. (**e**) Location of cysteine 234 in the PHGDH active site (PDB: 2G76). The C234S PHGDH mutation attenuates PHGDH inhibition by NCT-503. (**f**) Similar expression of PHGDH in MDA-MB-468 cells expressing wild-type and C234S PHGDH. Full gels are in Supplementary Fig. 8b. (**g**) NCT-502 decreases incorporation of U-^{13}C glutamine-derived carbon into α-ketoglutarate. (**h**) NCT-503 decreases incorporation of α–^{15}N glutamine-derived nitrogen into serine.

Supplementary Fig. 3. Additional PHGDH inhibitor efficacy data

a

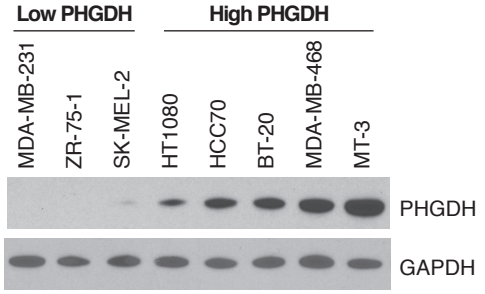

b

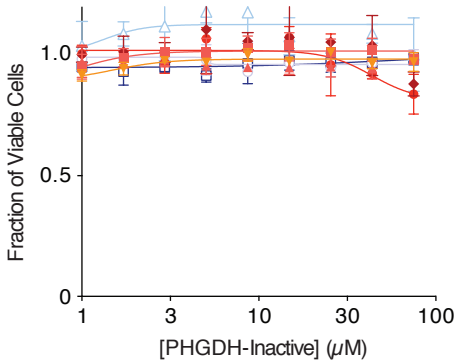

	PHGDH-Inactive EC_{50} (μM)
Low PHGDH	
MDA-MB-231	>100
ZR-75-1	>100
SK-MEL-2	>100
High PHGDH	
MDA-MB-468	>100
BT-20	>100
HCC70	>100
MT-3	>100
HT1080	>100

c

Compound	Structure	MDA-MB-468 EC_{50}, Cytotoxicity (μM)	MDA-MB-468 EC_{50} (Flux, μM)
NCT-503	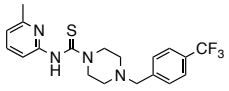	8	2.3
NCGC00356258	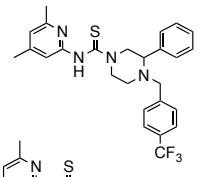	8.6	6.9
NCGC00356790	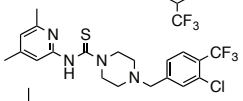	11	12.4
NCGC00356789	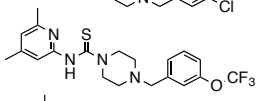	12.5	4.1
NCGC00356793	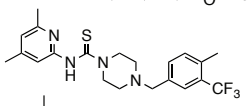	14.5	8.6
NCT-502	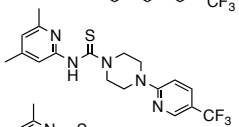	15.2	17.5
NCGC00351759	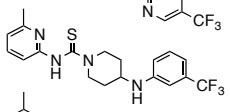	15.5	3.9
NCGC00356785	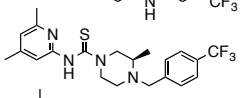	22.8	19.9
NCGC00356356	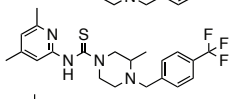	24.4	15.8
NGCC00356784	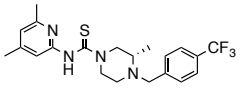	25.6	25.3
NCGC00351951	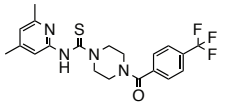	29.3	17

Supplementary Fig. 3 (continued). Additional PHGDH inhibitor efficacy data

d *In vivo* PK (30 mg/kg, IP, plasma)

Parameter	units	NCT-503
AUClast	hr*ng/mL	14700
SE_AUClast	hr*ng/mL	660
AUCINF_obs	hr*ng/mL	14700
AUC_%Extrap_obs	%	0.1
MRTINF_obs	hr	2.4
t1/2	hr	2.5
T_{max}	hr	0.083
C_{max}	ng/mL	7980

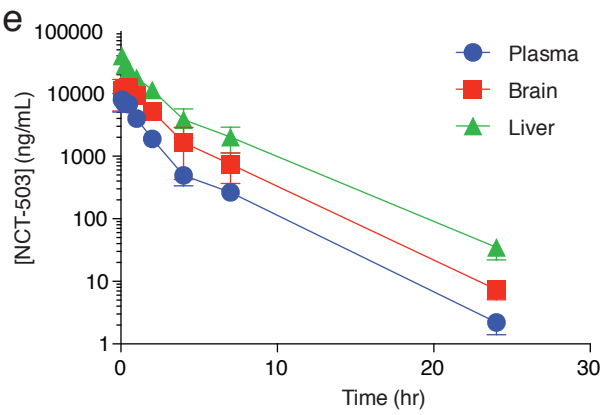

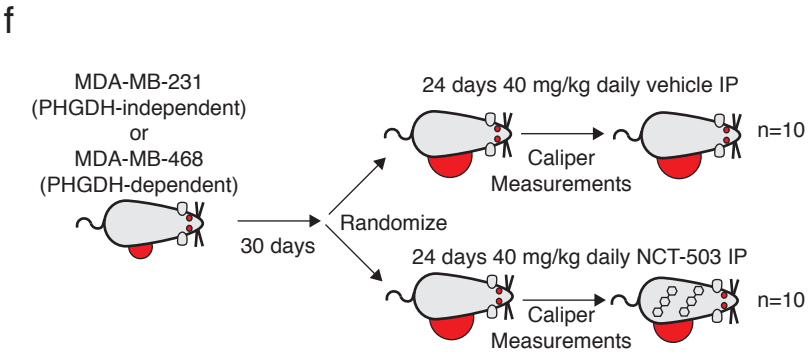

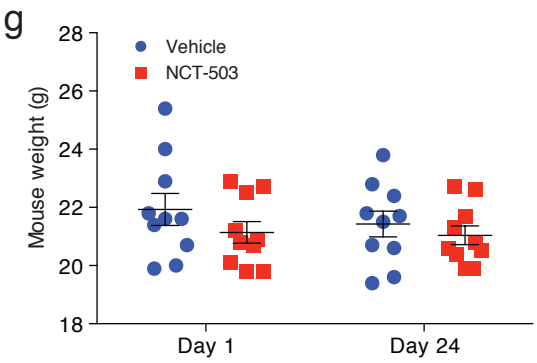

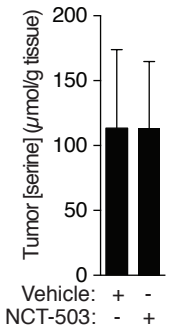

Supplementary Figure 3 | Additional PHGDH inhibitor efficacy data. (**a**) Western blot of PHGDH expression in tested cell lines. Full gels are in Supplementary Fig. 8c. (**b**) Inactive PHGDH inhibitor is not cytotoxic towards PHGDH-dependent or independent cell lines. Data are the mean of three biological replicates and error bars represent the standard deviation. (**c**) Compound structures and EC_{50}s for cytotoxicity and glucose to serine flux used for cytotoxicity-flux correlation (Fig. 3b). (**d**) Pharmacokinetic parameters of NCT-503 in plasma. Each point is the average of three experiments and error bars represent the standard deviation. (**e**) Pharmacokinetic profile of NCT-503 in plasma, liver and brain following a single 30 mg/kg IP administration. (**f**) Design of a mouse experiment to evaluate PHGDH inhibitor toxicity towards MDA-MB-468, PHGDH-dependent orthotopic xenografts with sparing of MDA-MB-231, PHGDH-independent orthotopic xenografts. (**g**) Mice treated with NCT-503 daily for 24 days do not lose weight relative to vehicle-treated mice. n=10 in each arm. Horizontal bars are the mean and error bars represent standard error of the mean. (**h**) MDA-MB-468 tumors from both treated and untreated mice have similar intraumoral serine concentrations. n=10 in each arm. Data are the mean and error bars represent the standard deviation.

Supplementary Fig. 4. PHGDH inhibition unexpectedly reduces the incorporation of exogenous serine into AMP and dTMP

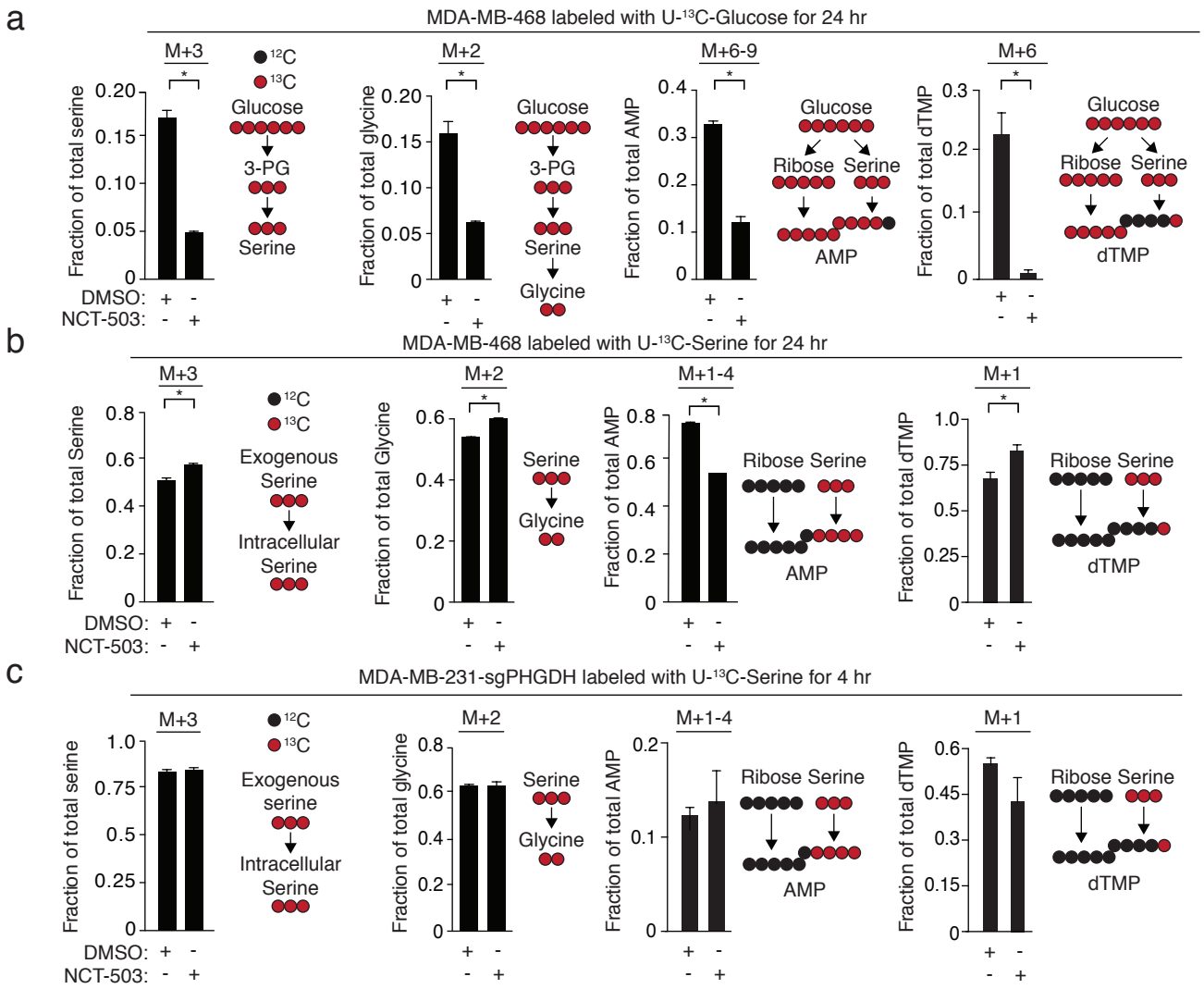

Supplementary Figure 4 | PHGDH inhibtion in a PHGDH-dependent cell line unexpectedly reduces the incorporation of exogenous serine into AMP and dTMP. All data presented are the mean of three independent biological replicates, and error bars represent the standard deviation. *, $p<0.05$, Student's *t*-test. (**a**) Treatment of MDA-MB-468 cells with 10 μM NCT-503 for 24 hours reduces the synthesis of glucose-derived serine and decreases ^{13}C incorporation, via serine, into AMP. In addition, ^{13}C from glucose-derived serine is not incorporated into dTMP. (**b**) 10 μM NCT-503 treatment for 24 hours in the presence of exogenous U-^{13}C-serine does not increase the proportion of labeled serine but increases the fraction of labeled glycine, consistent with decreased synthesis of unlabeled serine. NCT-503 reduces the incorporation of one-carbon units from exogenous U-^{13}C-serine into AMP and dTMP. The dTMP fractional labeling does not change greatly but the decrease in dTMP pool size (Supplementary Figs. 5d and 6b) decreases the accuracy of dTMP fractional labeling. (**c)** MDA-MB-231 cells lacking PHGDH do not exhibit an increase in M+2 glycine or a significant decrease in incorporation of exogenous serine into AMP or dTMP in the presence of 10 μM NCT-503.

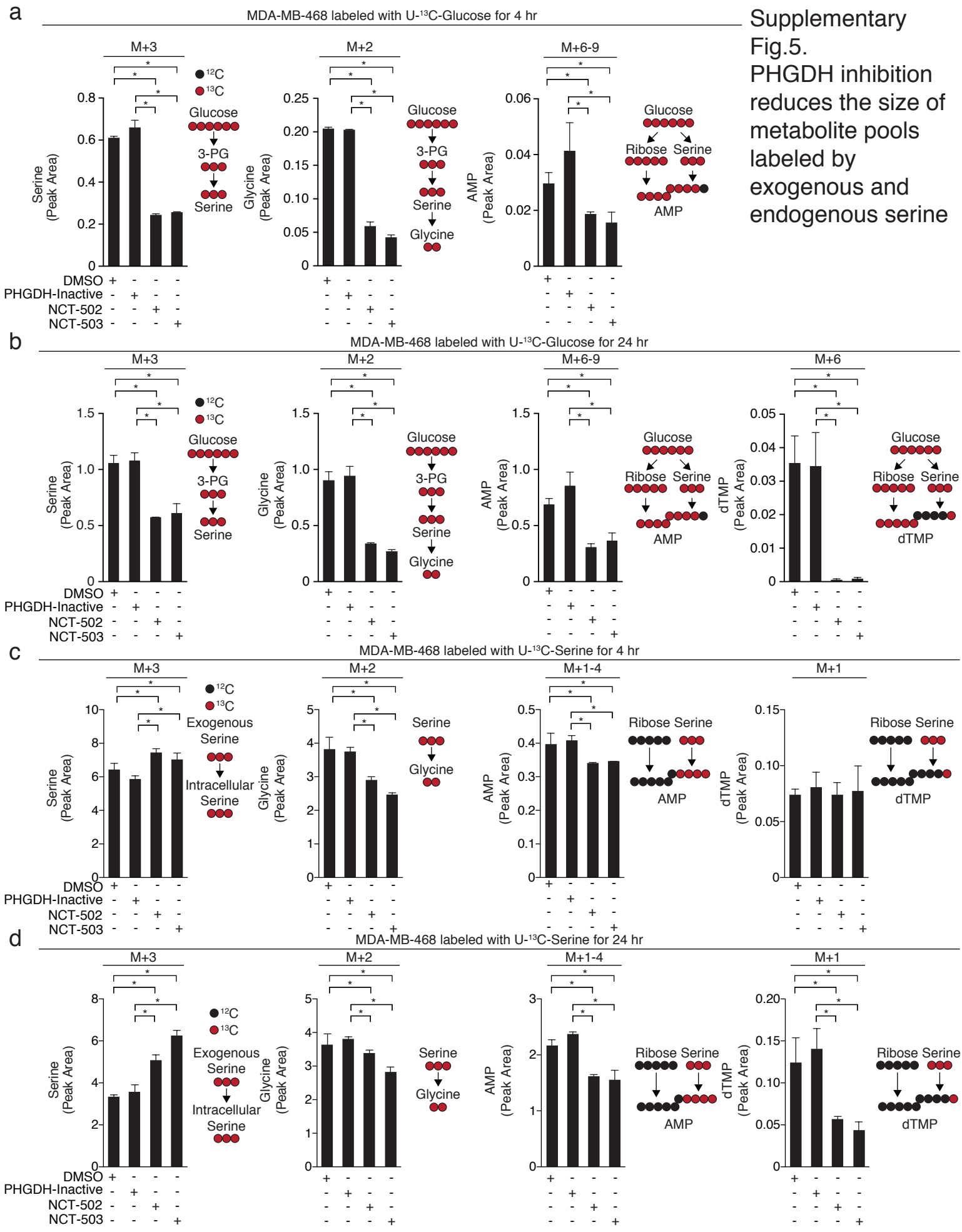

Supplementary Fig.5.
PHGDH inhibition reduces the size of metabolite pools labeled by exogenous and endogenous serine

Supplementary Figure 5 | PHGDH inhibition in a PHGDH-dependent cell line reduces the size of metabolite pools labeled by endogenous and exogenous serine. All data presented are the mean of three biological replicates and error bars represent the standard deviation. *, $p<0.05$, Student's *t*-test. All pools are normalized by total cell volume from an independently counted, identically treated plate. (**a**) Pools of M+3 serine, M+2 glycine, and M+6-9 AMP derived from U-^{13}C-glucose are unaffected by inactive compound but decrease in response to 10 μM NCT-502 or NCT-503 treatment. (**b**) The same results persist at 24 hours. In addition, 10 μM NCT-502 or NCT-503 both reduce the M+6 dTMP pool size. (**c)** Neither NCT-502 or NCT-503 affect the M+3 serine pool size at 4 hours, but both decrease the M+2 glycine and M+1-4 AMP pools. (**d**) At 24 hours, both 10 μM NCT-502 and NCT-503 significantly decrease the size of the M+1-4 AMP and M+1 dTMP pools generated by U-^{13}C-serine labeling.

Supplementary Fig. 6. Serine, glycine, AMP, and dTMP isotopomer distributions following PHGDH inhibitor treatment

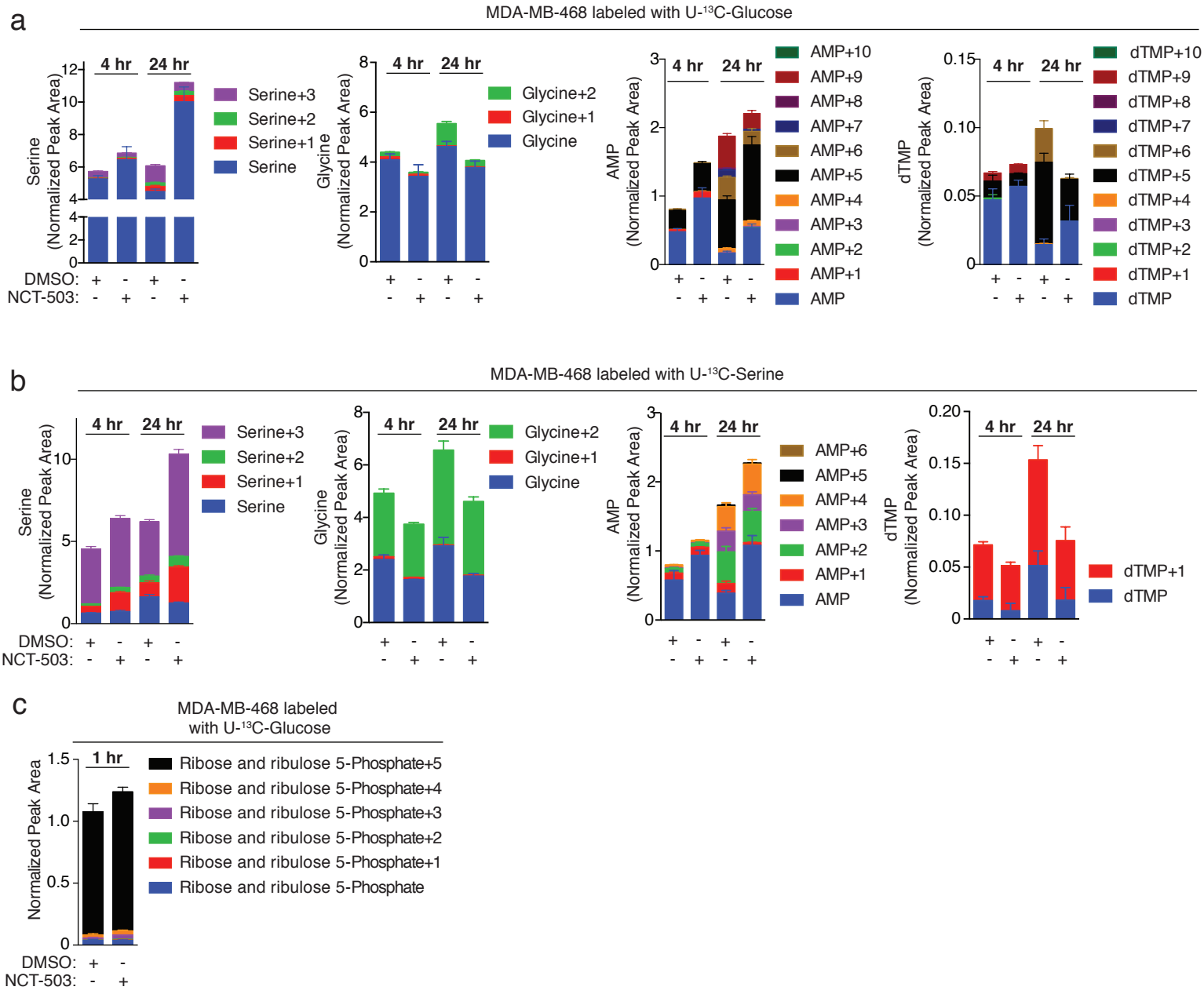

Supplementary Figure 6 | Isotopomer distributions of serine, glycine, AMP and dTMP following PHGDH inhibitor treatment. All data presented are the mean of three independent biological replicates and error bars represent the standard deviation. (**a**) Pool sizes following labeling with U-^{13}C glucose. Labeled serine and glycine decrease at 4 and 24 hours, and labeled and unlabeled dTMP pools decrease at 24 hours following NCT-503 treatment. (**b**) Pool sizes following labeling with U-^{13}C serine. Incorporation of ^{13}C into dTMP decreases at 24 hours following PHGDH inhibitor treatment. (**c**) Ribose and ribulose-5-phosphate pools following labeling with U-^{13}C-glucose. Both pentose pools increase at 1 hour following NCT-503 treatment.

Supplementary Fig. 7. Increased synthesis of serine from glycine following PHGDH inhibition.

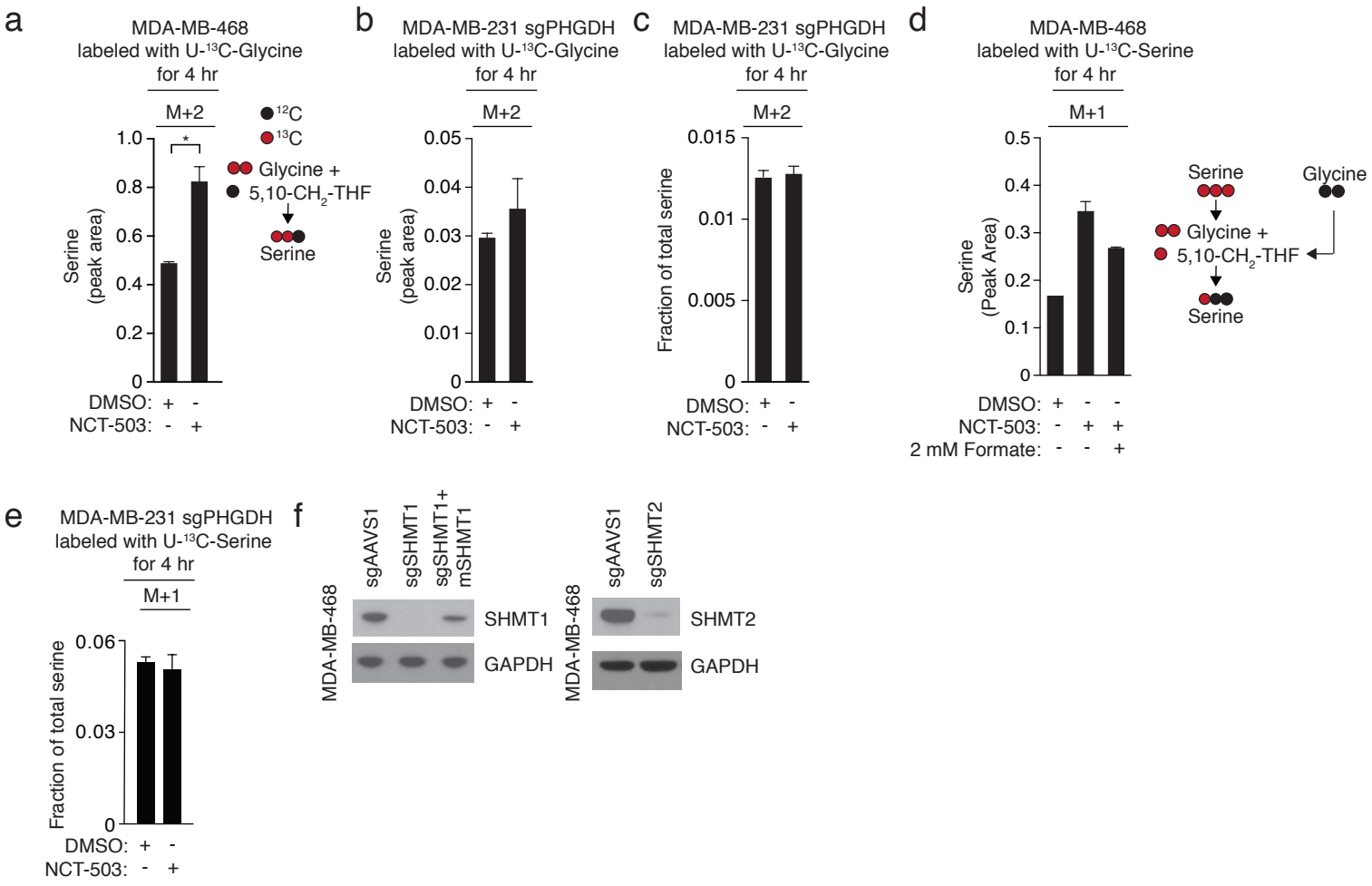

Supplementary Figure 7 | Increased synthesis of serine from glycine following PHGDH inhibition. All data presented are the mean of three independent biological replicates, and error bars represent standard deviations. *, $p<0.05$, Student's *t*-test. (**a**) Increased pool size of M+2 serine from U-^{13}C-glycine following PHGDH inhibitor treatment. (**b**) The M+2 glycine pool does not increase in MDA-MB-231 cells lacking PHGDH following NCT-503 treatment. (**c**) MDA-MB-231 cells lacking PHGDH do not fractionally label a large amount of M+2 serine from M+2 glycine following PHGDH inhibitor treatment. (**d**) Pool size data for likely SHMT1-mediated synthesis of M+1 serine from unlabeled glycine and ^{13}C-serine-derived 5,10 methylene THF (5,10-CH_2-THF), which increases with PHGDH inhibition (10 μM NCT-503) and is decreased by exogenous unlabeled formate. (**e**) NCT-503 does not induce increased M+1 serine labeling from M+3 serine in MDA-MB-231 cells lacking PHGDH. (**f**) Cas9 and sgRNA-mediated deletion of SHMT1 and SHMT2 in MDA-MB-468 cells, with rescue of SHMT1 expression with mouse SHMT1 (mSHMT1). Full gels are in Supplementary Figs. 8d-e.

Supplementary Fig. 8. Western blots

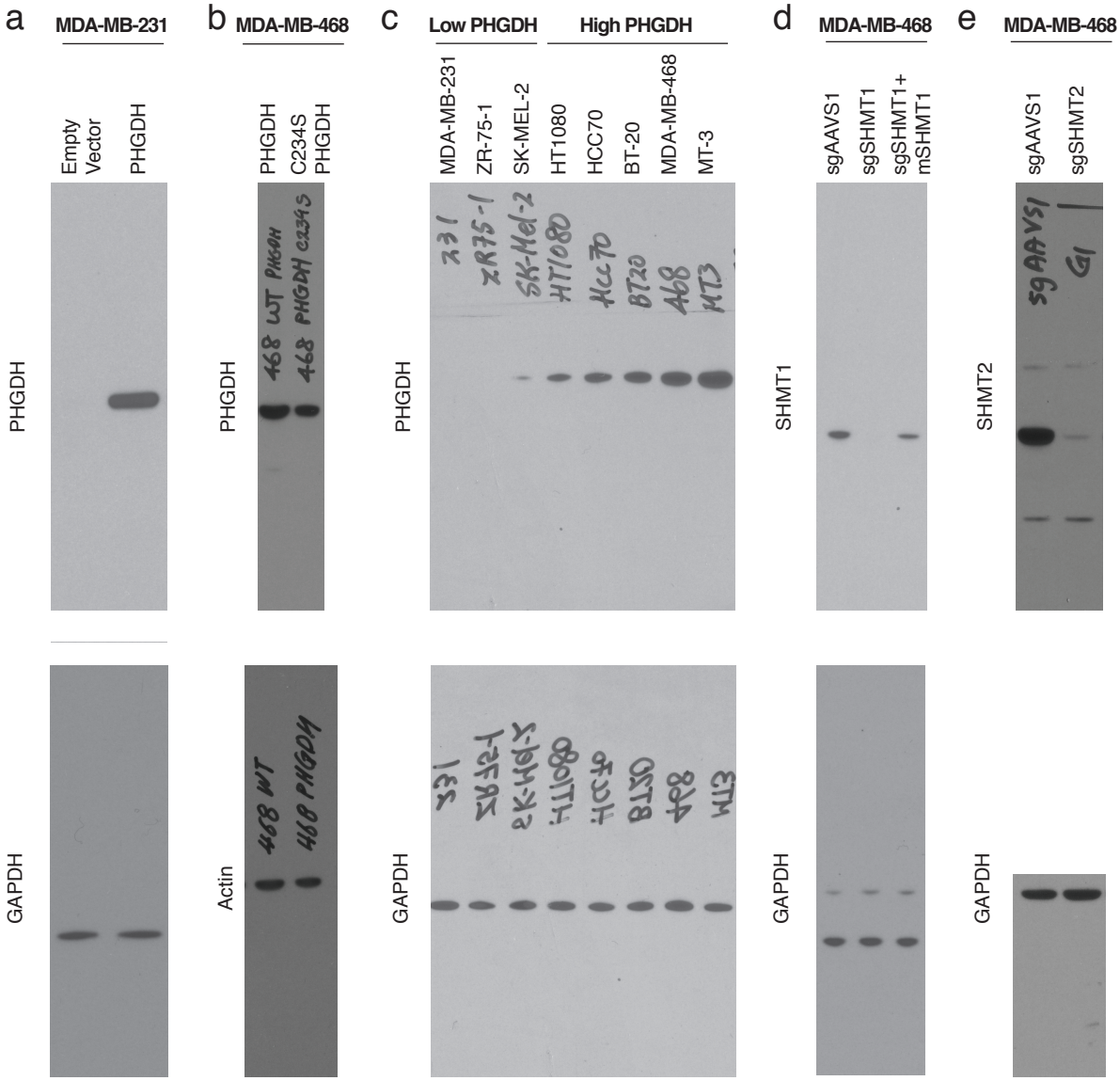

Supplementary Figure 8 | Western Blots. (**a**) Blot of PHGDH and GAPDH loading control demonstrating expression of PHGDH in MDA-MB-231 cells (Supplementary Fig. 2a). (**b**) Expression of wild-type and C234S PHGDH in MDA-MB-468 cells with actin as a loading control (Supplementary Fig. 2f). (**c**) Blot of PHGDH showing differential expression of PHGDH in multiple cell lines with GAPDH as a loading control (Supplementary Fig. 3a). (**d**) Blot of human SHMT1 in MDA-MB-468 cells expressing sgRNAs against AAVS1 or SHMT1, with the addition of Cas9-resistant mouse SHMT1, with GAPDH as the loading control (Supplementary Fig. 7f). (**e**) Blot of SHMT2 in MDA-MB-468 cells with sgRNA against AAVS1 or SHMT2, with GAPDH as the loading control (Supplementary Fig. 7f).

Supplementary Fig. 9. Purification of PHGDH, PSAT1 and PSPH

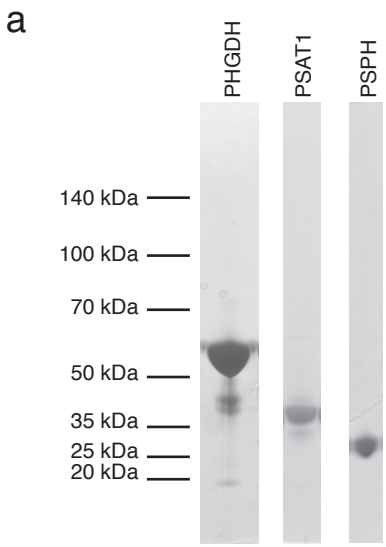

Supplementary Figure 9 l Purification of PHGDH, PSAT1, and PSPH. (**a**) PHGDH, PSAT1 and PSPH were purified to homogeneity by immobilized metal affinity chromatography (Ni^{2+}) and size exclusion chromatography.